Chapter 5
Insights of MILD Combustion from High-Fidelity Simulations

Hang Zhou, Josh McConnell, Terry A. Ring, and James C. Sutherland

Abstract Simulation of coal combustion remains challenging due to the many physical processes involved which span a large range of length and time scales. Although detailed models exist for devolatilization, char oxidation and gas-phase kinetics, most simulation efforts simplify these models considerably to reduce the high cost of simulation. Three mixture fraction-based chemistry models are evaluated, namely, the steady laminar flamelet, equilibrium, and Burke-Schumann models in the scope of coal volatiles combustion. Coal volatiles are assumed to be composed of "light gasses" (CH_4, CO, etc.) as well as tar, which refers to the various large aromatic compounds released during the devolatilization process. Here, tar is treated as a single empirical species. Each mixture fraction-based model is evaluated by comparing predicted gas phase properties to computations using finite-rate chemistry with a detailed reaction model. The results indicate that the reconstructions for gas phase temperature and composition from steady flamelet model is the most accurate. The Burke-Schumann chemistry model performed very poorly for predicting the gas phase temperature and composition under stoichiometric conditions. We apply the steady laminar flamelet model to Moderate or Intense Low Oxygen Dilution (MILD) combustion. A key requirement for MILD combustion is that mixing rates are sufficiently fast that gas-phase chemistry occurs nearly volumetrically, eliminating visible flame structures. A Well-stirred reactor assumption is applied to MILD combustion due to its characteristic of volumetric reactions. The necessary conditions to achieve MILD combustion, including recirculation rate of flue gas and heat loss, are determined under various mixture fractions and mass fractions of light gas in the fuel stream. We conclude that the increasing the recirculation rate and heat loss are helpful for achieving MILD regime. Additionally, we observe that the recirculation rate and heat loss values required to achieve MILD combustion increase as the fuel stream is enriched in light gases. Steady flamelet computations reveal that

H. Zhou · J. McConnell · T. A. Ring · J. C. Sutherland (✉)
Department of Chemical Engineering, The University of Utah, Salt Lake City, UT, USA
e-mail: James.Sutherland@utah.edu

MILD combustion can be achieved when reactants are not well-mixed as long as the scalar dissipation rate is sufficiently large. Our considerations indicate that the steady laminar flamelet model provides a reliable method to model MILD combustion in the absence of well-mixed reactants.

Keywords High-fidelity simulation · Coal combustion · Mixture fraction-based models · MILD

5.1 Introduction

Coal combustion involves a variety of highly-coupled, complex phenomena that span a large range of spatial and temporal scales such as thermochemistry and turbulence in the fluid phase, as well as vaporization, devolatilization, heterogeneous reactions in the particle phase. Direct numerical simulation (DNS) and large-eddy simulation (LES) are useful computational tools for studying the physical processes that occur during the in coal combustion process, and a number of computational studies have been undertaken using these two approaches (Rieth et al. 2018; Bai et al. 2016; Hara et al. 2015; Watanabe and Yamamoto 2015; Zhou 2019). However, simplified methods are often used for gas phase reaction kinetics, devolatilization, and char oxidization, such as the two-step devolatilization model (Rieth et al. 2018; Luo et al. 2012) and kinetic/diffusion model for char oxidization (Watanabe and Yamamoto 2015), in order to reduce the computational burden of performing simulations. Therefore, finding a high-fidelity model that is capable of balancing the accuracy of resolving complex coal combustion process with simulation cost becomes a critical step.

The One-Dimensional Turbulence (ODT) model proposed by Kerstein (1999) provides the ability to resolve the full range of length and time scales as in DNS at a substantially lower computational cost. The ODT model represents a line of sight through a three-dimensional turbulent flow field, in which the size and frequency of mixing events are determined by the local fluid dynamics. Past work has demonstrated that one-dimensional approaches to combustion simulation are capable of accurately predicting ignition delay (Goshayeshi and Sutherland 2014), flame stand-off (Goshayeshi and Sutherland 2015a, b) as well as char burnout (McConnell et al. 2016, 2017), and have been used as a cost-effective method for combustion models spanning a wide range of physical fidelity. In this work, the ODT model is used as means to generate data using advanced combustion models.

To ensure that calculations are tractable, simplified chemistry models are often employed, typically parameterized by one or more mixture fractions in conjunction with other parameters such as normalized heat loss. Pedel et al. (2013) utilize a mixture fraction approach with equilibrium chemistry in a study of the ignition behavior in a semi-industrial coal furnace. In a study by Olenik and coworkers (2015), gas phase properties are determined by calculating the state among 6 species. A more recent development is the application of laminar flamelet models to coal combustion. Studies undertaken by Watanabe and Yamamoto (2015) and Rieth et al. (2016)

model gas phase chemistry using a flamelet model parameterized with two mixture fractions corresponding to the products of devolatilization char oxidation. Another work outlined in Watanabe et al. (2017) extends the flamelet approach described in Watanabe and Yamamoto (2015) to include consideration of a mixture fraction for moisture to account for the effects of water evaporation that occurs as coal is heated. More recently, Wen et al. (2019) perform an a priori analysis of the flamelet model for a laminar coal flame near an isothermal wall and find that the flamelet model is able to reproduce the thermochemical state accurately. Furthermore, a study by McConnell and Sutherland (2020) develop a practical approach to joining an empirical tar and soot model to a steady flamelet model and and examine the impact of the required modeling assumptions through an a priori comparison to data generated using a finite rate chemistry model. To evaluate the accuracy of various simplified chemistry models, three mixture fraction-based models are applied in this work.

MILD combustion has attracted increased attention in recent years because of its high efficiency and low emissions. To attain these characteristics, the main criteria of MILD combustion needed to be satisfied are that the inlet temperature of the reactant mixture is higher than mixture self-ignition temperature, and the maximum allowable temperature increase with respect to inlet temperature during combustion is lower than mixture self-ignition temperature (in Kelvin) (Cavaliere and De Joannon 2004). Strong turbulent intensity is always applied to increase the recirculation of high temperature flue gases to dilute and preheat the reactants prior to combustion. However, simulation of coal combustion with strong turbulent intensity using detailed kinetics for gas phase and coal devolatilization models remains difficult due to the high computational cost. In the present investigation, studies of MILD combustion using solid fuels, such as pulverized coal, are still limited (Weber et al. 2005; Li 2014; Smart and Riley 2012). Saha et al. (2013, 2014, 2015, 2016, 2017) have carried out several studies investigating the effect of particle size, turbulence, and coal type on MILD combustion using pulverized coal in a self-recuperative furnace. However, the existence of "ghost flames" or sparks caused by poor mixing between volatile matter and the surrounding hot combustion products was reported in all of these papers. This conflicts with the MILD combustion characteristic of invisible flames. This indicates that it is difficult to attain well-mixedness in a combustion reactor, especially around the pulverized coal particles. On the other hand, OH Planar Laser Induced Fluorescence (PLIF) images from experiments indicate the presence of thin reaction zones where MILD combustion is observed (Wunning and Wunning 1997; Özdemir and Peters 2001; Weber et al. 2005), conflicting with the characteristic of distributed reaction zone for MILD combustion. This observation demonstrates that the conditions required for MILD combustion, such as well-mixedness, are not well-characterized for solid fuels such as coal.

In this work, we first perform an a priori assessment of the predictive capability of three mixture fraction-based modeling approaches, specifically, the steady laminar flamelet, equilibrium, and Burke-Schumann chemistry models in the scope of coal volatiles combustion with consideration of a tar and soot formation model. We subsequently investigate the required conditions to obtain MILD combustion, including recirculation rate and heat loss. Requirements to attain MILD combustion are deter-

mined over a large range of oxidizer/fuel mixtures as well as a fuel composition
with a various light gas to tar ratios. These requirements are investigated under the
assumption of a perfectly-mixed system using a a well-stirred reactor model, whereas
poorly-mixed conditions are investigated using the steady laminar flamelet model.
Results from the steady laminar flamelet model are compared with the those from the
well-stirred reactor model to evaluate the effects of the main parameters, including
recirculation rate and heat loss on the achievement of MILD regime and its efficacy
to model MILD combustion. The insight provided in this study should help guide
the setup of experimental conditions to achieve MILD combustion.

5.2 Theoretical Formulation

5.2.1 Governing Equations for Coal Combustion Simulation

In each simulation, the gas and particle phases are evolved in Eulerian and Lagrangian
frames of reference, respectively.

5.2.1.1 Gas Phase

The gas phase conservation equations are written as (Goshayeshi and Sutherland
2014, 2015a)

$$\frac{\partial \rho \varphi}{\partial t} = -\frac{\partial \rho \varphi v}{\partial y} - \frac{\partial \Theta_\varphi}{\partial y} + \omega_\phi + \sum_{j=1}^{n_p} \frac{S_{p_j \varphi}}{V_{cell}}, \tag{5.1}$$

where φ is an intensive quantity, Θ_φ is the diffusive flux of φ, ω_φ is the net rate of
production of φ in the gas phase, V_{cell} is the quantity representing the volume of the
control volume, and $S_{p_j \varphi}$ is gas-phase source term for φ from the particle phase. In
this formulation, $\varphi = \{1, u, v, e_0, Y_i\}$ where ρ is the mass density, u and v are the x
and y components of velocity, respectively, e_0 is the specific total internal energy, and
Y_i are species mass fractions. For the continuity equation, $\varphi = 1$ and $\Theta_\rho = 0$. The set
of equations defined by (5.1) are closed using the ideal gas equation, $P = \rho RT/M$,
and the following relationships are used for the diffusive fluxes for momentum and
energy:

$$\Theta_v = \tau_{yy} + P = -\frac{4}{3}\mu \frac{\partial v}{\partial y} + P, \tag{5.2}$$

$$\Theta_u = \tau_{yx} = -\mu \frac{\partial u}{\partial y}, \tag{5.3}$$

$$\Theta_{e_0} = -\kappa \frac{\partial T}{\partial y} + \sum_{i=1}^{n_s} h_i \Theta_{Y_i}, \tag{5.4}$$

where μ is the viscosity, κ is the thermal conductivity, and n_s is the number of species, and h_i is the enthalpy of species i.

To investigate the impact of differential diffusion on model accuracy, two different forms of the species diffusive flux are implemented. The first assumes uniform diffusivity, D, across all species:

$$\Theta_{Y_i} = -\rho D \frac{\partial Y_i}{\partial y}, \tag{5.5}$$

where D is set based on the assumption that all species have a unity Lewis number, i.e.

$$D_i = \frac{\kappa}{\text{Le}_i \rho c_p} = \frac{\kappa}{\rho c_p}, \tag{5.6}$$

where c_p is the heat capacity. The second form of the species diffusive flux implemented is given as

$$\Theta_{Y_i} = -\frac{\rho Y_i}{X_i} D_i \frac{\partial X_i}{\partial y}, \tag{5.7}$$

where X_i and D_i are the mole fraction and mixture-averaged diffusivity of species i.

Turbulent mixing is modeled using the One-Dimensional Turbulence (ODT) model. ODT models mimic turbulent mixing through instantaneous rearrangement of adjacent fluid parcels (eddy events). By construction, the ODT model conserves momentum, energy, and mass over the interval of the eddy event (Kerstein 1999; Sutherland et al. 2019). The size, duration, and location of each eddy event are determined by the local properties of the flow field, which allows ODT to capture the $-5/3$ energy cascade inherent to isotropic turbulence (Kerstein 1999; Sutherland et al. 2019). For details of the ODT model, the reader is referred to Kerstein (1999), Sutherland et al. (2019).

A model based on the GRI 3.0 mechanism (Lu and Law 2008) consisting of 184 reactions among 30 species is used as a basis for calculating species source terms, ω_{Y_i}.

5.2.1.2 Particle Phase

In this work, only mass loss by devolatilization is considered, so conservation equations for particle phase quantities do not include terms for evaporation or char consumption. Therefore, conservation equations for the mass, velocity, and temperature of each particle are given as

$$\frac{dm_{\text{p}}}{dt} = \frac{dm_v}{dt}, \tag{5.8}$$

$$\frac{\mathrm{d}u_\mathrm{p}}{\mathrm{d}t} = \frac{g_x(\rho_\mathrm{p} - \rho_\mathrm{g})}{\rho_\mathrm{p}} + S_\mathrm{p,u}, \tag{5.9}$$

$$\frac{\mathrm{d}v_\mathrm{p}}{\mathrm{d}t} = \frac{g_y(\rho_\mathrm{p} - \rho_\mathrm{g})}{\rho_\mathrm{p}} + S_\mathrm{p,v}, \tag{5.10}$$

$$\frac{\mathrm{d}T_\mathrm{p}}{\mathrm{d}t} = \frac{A_\mathrm{p}}{m_\mathrm{p}C_\mathrm{p}} \left[h_c \left(T_\mathrm{p} - T_\mathrm{g} \right) + \epsilon_\mathrm{p}\sigma \left(T_\mathrm{p}^4 - T_\mathrm{w}^4 \right) \right], \tag{5.11}$$

where m_p and m_v are the total and volatile mass of the particle, respectively, u_p and v_p are the x and y components of the particle velocity, respectively, u_g and v_g are the x and y components of the gas velocity, respectively. T_p, A_p, ρ_p, C_p, and ϵ_p are the particle temperature, surface area, density, heat capacity, and emissivity, respectively, ρ_g is the gas density, T_wall is a furnace "wall" temperature, σ is the Stefan-Boltzmann constant, and $h_c = Nu\kappa/d_\mathrm{p}$ is a convective heat transfer coefficient where $Nu = 2 + 0.6Re_\mathrm{p}^{1/2}Pr^{1/3}$ and d_p is the particle diameter.

In this work, two devolatilization models are considered. The first is the Chemical Percolation and Devolatilization (CPD) model described in Jupudi et al. (2009), Goshayeshi and Sutherland (2014, 2015a). For devolatilization, we consider a modified form of the Chemical Percolation and Devolatilization (CPD) model described in Jupudi et al. (2009), Goshayeshi and Sutherland (2014, 2015a) in which speciation of coal volatiles is disabled, and referred to as CPD-NS henceforth. The CPD-NS model uses the following definition for species devolatilization rates:

$$\left(\frac{\mathrm{d}m_{v,i}}{\mathrm{d}t} \right)^{\mathrm{CPD\text{-}NS}} = Y_{v,i}^0 \left(\frac{\mathrm{d}m_v}{\mathrm{d}t} \right)^{\mathrm{CPD}}, \tag{5.12}$$

where $m_{v,i}$ is the mass of species i in the coal volatiles and $Y_{v,i}^0$ is the initial mass fraction of species i in the coal volatiles.

As implemented, the CPD-NS model assumes that the coal volatiles are composed of CH_4, CO, CO_2, H_2, and H_2O, and tar. NH_3 and HCN, which are additional products of devolatilization considered in the formulation of the CPD model, are not considered here as neither of these species are included in the gas phase kinetic mechanism implemented in this work.

5.2.1.3 Tar and Soot Treatment

In this work, we consider a treatment of coal-derived tar and soot based on the model developed by Brown and Fletcher (1997), in which tar is assumed to be a high molecular weight hydrocarbon and soot is assumed to be composed of carbon. We assume tar and soot do not affect the thermodynamic properties of the system directly and only interact with the system through reactive source terms. Herein, we assume that tar is dihydronaphthalene ($C_{10}H_{10}$) and further assume that soot has the same empirical formula as tar, which results in the following reaction scheme

$$\text{tar} \rightarrow \text{soot},$$
$$\text{tar} + O_2 \rightarrow CO + H_2O,$$
$$\text{soot} + O_2 \rightarrow CO + H_2O. \tag{5.13}$$
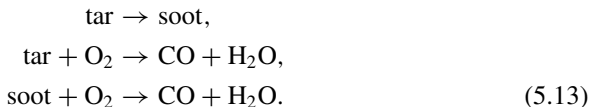
The primary motivation for assuming soot has the same stoichiometry as tar is that the product composition resulting from (5.13) can be parametrized by a single stream, whereas three streams are required to adequately parameterize tar and soot reactions if soot is assumed to be carbon. This modification of the Brown-Fletcher tar and soot approach ensures that implementation of the mixture fraction-based models described in Sect. 5.2.2 remains tractable. It has been demonstrated that the steady laminar flamelet model is capable of providing an accurate a priori prediction of gas composition and temperature by assuming the same stoichiometry for tar and soot (McConnell and Sutherland 2020).

5.2.2 Mixture Fraction Based Models

One of the goals of this study is to assess the performance of three mixture fraction based chemistry models. What follows is a concise description of each of the considered modeling approaches.

All models are parameterized by Z_{lg}, Z_{tp}, and γ, where Z_{lg} and Z_{tp} are mixture fractions for volatile light gases and reaction products of tar and soot oxidation, respectively, and γ is the normalized heat loss. The flamelet model described in Sect. 5.2.2.3 is parameterized by an additional variable, χ_{max}, which is the scalar dissipation rate. The total mixture fraction, Z, is given by

$$Z = Z_{lg} + Z_{tp}, \tag{5.14}$$

where

$$Z_{lg} = \frac{M_{lg}}{M_{lg} + M_{tar} + M_{ox}}, \tag{5.15}$$

$$Z_{tp} = \frac{M_{tp}}{M_{lg} + M_{tar} + M_{ox}}. \tag{5.16}$$

M_{lg} and M_{tar} are masses originating from light gases in the coal volatiles and tar, respectively, M_{tp} is the mass of CO, H_2O, and N_2 supplied to the system through reaction of tar and soot and M_{ox} is the mass originating from the oxidizer, which for this study, is air. The mixture fractions Z_{lg} and Z_{tp} are obtained by performing a linear best-fit analysis on elemental mass balance equations:

$$E_i = Z_{lg} E_{i,lg} + Z_{tp} E_{i,tp} + \left(1 - Z_{lg} - Z_{tp}\right) E_{i,ox} \tag{5.17}$$

with $i = \{C, H, O\}$. E_i, $E_{i,\text{lg}}$, $E_{i,\text{tp}}$, and $E_{i,\text{ox}}$ are the mass fractions of element i obtained from simulation data, in the volatile light gas stream, in the tar product stream, and in the oxidizer stream, respectively. The parameter ζ is the fraction of fuel mass originating from volatile light gases given by

$$\zeta = \frac{Z_{\text{lg}}}{Z_{\text{lg}} + Z_{\text{tp}}}. \tag{5.18}$$

The variable ζ is used to parameterize fuel-side boundary for each model; $\zeta = 1$ indicates all fuel originates from volatile light gases and $\zeta = 0$ indicates all fuel originates from tar and soot combustion products. The normalized heat loss, γ, is determined through the following expression

$$\gamma = \frac{h_{\text{ad}} - h_{\text{sim}}}{h_{\text{ad}} - h(T_{\text{g,ref}})}, \tag{5.19}$$

where $h_{\text{ad}} = Z_{\text{lg}}h_{\text{lg}}(T_{\text{lg}}) + Z_{\text{tp}}h_{\text{tp}}(T_{\text{tp}}) + (1 - Z_{\text{lg}} - Z_{\text{tp}})h_{\text{ox}}(T_{\text{ox}})$ is the adiabatic mixture enthalpy where h_{lg}, h_{tp} and h_{ox} are the enthalpy of volatile light gas, tar products and oxidizer streams, respectively, and T_j, $j = \{\text{lg, tp, ox}\}$ are the stream temperatures. The values h_{sim} and $T_{\text{g,sim}}$ are the gas phase enthalpy and temperature, respectively, obtained from simulation data, $T_{\text{g,ref}} = 298$ K is the reference temperature, and $h(T) = Z_{\text{lg}}h_{\text{lg}}(T) + Z_{\text{tp}}h_{\text{tp}}(T)(1 - Z_{\text{lg}} - Z_{\text{tp}})h_{\text{ox}}(T)$ for $h(T_{\text{g,ref}})$.

5.2.2.1 Burke-Schumann Chemistry

The Burke-Schumann model (1928) assumes an infinitely-fast reaction between fuel and oxidizer, where CO_2, H_2O, and N_2 are the products of combustion. The gas composition according to the Burke-Schumann model is given by

$$Y_i = \begin{cases} Y_{i,\text{O}} + \frac{Z}{Z_{\text{st}}}\left(Y_{i,\text{st}} - Y_{i,\text{O}}\right) & Z \leq Z_{st} \\ Y_{i,\text{F}} + \frac{1-Z}{1-Z_{\text{st}}}\left(Y_{i,\text{st}} - Y_{i,\text{F}}\right) & Z > Z_{\text{st}} \end{cases}, \tag{5.20}$$

where $Y_{i,\text{O}}$, $Y_{i,\text{F}}$, and $Y_{i,\text{st}}$ are the mass fractions of species i in the oxidizer stream, fuel stream, and at stoichiometric conditions, and Z_{st} is the stoichiometric mixture fraction.

The mixture enthalpy, h, is given in terms of the heat loss parameter as

$$h = (1 - \gamma)h_{\text{ad}} + \gamma h_{\text{ref}}. \tag{5.21}$$

Temperature is obtained using the Cantera software package (Goodwin et al. 2017) by specifying the enthalpy, pressure, and composition.

5.2.2.2 Equilibrium Chemistry

Like the Burke-Schumann model, the equilibrium model assumes infinitely-fast chemical kinetics. Rather than assuming complete combustion of fuel, the product composition for the equilibrium model is set based on a suitable reaction mechanism. In this work, equilibrium composition and temperature are obtained with the same chemical mechanism (Lu and Law 2008) used to generate simulation data using the Cantera software package (Goodwin et al. 2017).

5.2.2.3 Steady Laminar Flamelet

Unlike the Burke-Schumann and equilibrium models, the steady laminar flamelet model accounts for the effect of diffusion on the chemical state. The temperature and composition are determined by solving the following system of ODEs

$$\frac{\chi}{2\mathrm{Le}_i}\frac{\mathrm{d}^2 Y_i}{\mathrm{d}Z^2} = -\frac{1}{\rho}\omega_{Y_i}, \tag{5.22}$$

$$\rho c_p \frac{\chi}{2}\frac{\mathrm{d}^2 T}{\mathrm{d}Z^2} = \sum_{j=1}^{n_s} h_j \omega_{Y_j} - \omega_h, \tag{5.23}$$

where

$$\chi = \chi_{\mathrm{max}}\exp\left(-2\left[\mathrm{erf}^{-1}(2Z-1)\right]^2\right), \tag{5.24}$$

as suggested in Peters (1984), and Le_i is the Lewis number for species i. The quantity ω_h is an energy source term chosen included for the purpose of generating non-adiabatic flamelet solutions and is set to

$$\omega_h = H(T - T_{\mathrm{conv}}), \tag{5.25}$$

where T_{conv} is chosen to be $T_{\mathrm{ad}} + \Delta T$, T_{ad} is the adiabatic flamelet temperature, and ΔT is set to $(\pm)2000$ K for solutions corresponding to positive and negative values of γ, respectively. Boundary conditions for (5.22) and (5.23) are set using the following formulae

$$Y_i(Z=0) = Y_{\mathrm{ox},i}, \tag{5.26}$$

$$Y_i(Z=1) = \zeta Y_{\mathrm{lg},i} + (1-\zeta)Y_{\mathrm{tp},i}, \tag{5.27}$$

$$T(Z=0) = T_{\mathrm{ox}}, \tag{5.28}$$

$$T(Z=1) = T \text{ such that } h(T) = \zeta h_{\mathrm{lg}}(T_{\mathrm{lg}}) + (1-\zeta)h_{\mathrm{tp}}(T_{\mathrm{tp}}), \tag{5.29}$$

where the light gas (lg) and tar products (tp) temperatures are determined using

$$T_{\mathrm{lg}} = -\frac{\sum_j^{n_p} \int_0^\infty \frac{dm_{v,j}}{dt} T_{\mathrm{p}} dt}{\sum_j^{n_p} m_{v,j}},$$

(5.30)

$$T_{\mathrm{tp}} = \frac{\int_0^\infty \left(\omega_{\mathrm{tar},ox} + \omega_{\mathrm{soot},ox}\right) T_g dt}{\int_0^\infty \left(\omega_{\mathrm{tar},ox} + \omega_{\mathrm{soot},ox}\right) dt},$$

(5.31)

where $\omega_{\mathrm{tar},ox}$ and $\omega_{\mathrm{soot},ox}$ are the tar and soot oxidation rates, respectively.

5.2.3 Well-Stirred Reactor Models

In MILD combustion, high turbulent intensity is required for rapid dilution and high temperature of the reactants. This leads to high mixing rate and lower temperature in the reactor, which subsequently leads to lower chemical reaction rates. These two main characteristics suggest the use of well-stirred reactors to model MILD gas-phase combustion (Cavaliere and De Joannon 2004; Plessing et al. 1998), which provides a perfectly mixed, volumetric reaction environment.

The well-stirred reactor model in this work assumes an open, rigid perfectly-stirred spherical vessel with radius r at constant pressure p. In the present study, the volatiles, including the volatile light gases and reaction products of tar and soot oxidation, produced from coal particles are used as the fuel, and no particle is considered. The equations solved for this reactor with residence time $\tau_{\mathrm{mix}} = V/\dot{V}_{\mathrm{in}}$ are

$$\frac{dY_i}{dt} = \frac{\rho_{\mathrm{in}}}{\rho \tau_{\mathrm{mix}}} (Y_{i,\mathrm{in}} - Y_i) + \frac{\dot{\omega}_i}{\rho},$$

(5.32)

$$\frac{dh}{dt} = \frac{\rho_{\mathrm{in}}}{\rho \tau_{\mathrm{mix}}} (h_{\mathrm{in}} - h) - \frac{3k}{\rho r}(T - T_{\mathrm{inf}}),$$

(5.33)

where ρ is the density, h is the enthalpy of the gas phase, Y_i is the species mass fraction, $\dot{\omega}_i$ is the volumetric species chemical reaction rate and k is the convective heat transfer coefficient, which considers the convective heat transfer between gas and surroundings with temperature T_{inf}. The "in" subscript indicates an inlet (feed) condition. The Dual-Time stepping method described in Hansen and Sutherland (2017) is used to provide an efficient, robust solution of these equations.

In industrial scale reactors, it is difficult to obtain the required turbulent intensity for perfectly mixed reactants throughout the whole reactor due to the limitations of the equipment. Different amounts of flue gas are recirculated and are mixed with the local reactants in various locations of the reactor to get well-mixed reactants locally. To mimic the reactions in various locations, well-stirred reactors with various mixture fractions, heat losses and recirculation rates are applied in this work. To analyze the degree of dilution of the reactants due to the recirculation of flue gas in MILD combustion, Wunning and Wunning (1997) define the recirculation rate (K_v) as

$$K_v = \frac{\dot{m}_e}{\dot{m}_o + \dot{m}_f} \tag{5.34}$$

where, $\dot{m}_e$, $\dot{m}_o$ and $\dot{m}_f$ are the mass flow rate of entrained flue gas, initial oxidizer and initial fuel respectively. To mimic the heat loss of the gas phase, the definition for normalized heat loss in (5.19) is applied. Considering the transient changing process of light gases and tar products, different values of ζ are used to get the oxidizer temperature and fuel temperature and composition based on Eq. (5.18).

5.3 Computational Configuration

In this work, the data used as a basis for a priori assessment of chemistry models was generated through simulation of a turbulent coal combustion simulation system consistent with high temperature air combustion (HiTAC) conditions (Suda et al. 2002; Tamura et al. 2015). For the ODT calculation, a domain with length 0.2 m is initialized to a temperature and composition consistent with air at 1200 K. Air at 1200 K as well as coal particles with a diameter of 50 µm and temperature of 350 K are injected though a nozzle with a diameter of 15.8 mm at the center of the domain at a velocity of 14.92 m/s. Velocity over the remainder of the domain is set to zero. The governing equations are solved using a fully-coupled scheme with a first-order explicit time integration scheme, a second-order spatial discretization, and characteristic boundary conditions Sutherland and Kennedy (2003). The spatial and temporal resolutions of 200 µm and 50 ns, respectively, are used to obtain a solution to the numerical system.

The Illinois #6 coal is considered in this work, with proximate and ultimate analyses given in Tables 5.1 and 5.2. The composition of coal volatiles is given in Table 5.3. The composition of the coal volatiles was determined using a 2D interpolation technique based on molar O/C and H/C ratios from the Illinois #6 coal and data from library coals (Zhao et al. 1994).

Table 5.1 Proximate analyses of the Illinois #6 coal

Proximate %			
Moisture	Ash	Volatiles	Fixed C
0.0	8.86	40.70	50.44

Table 5.2 Ultimate analyses of the Illinois #6 coal

Ultimate (dry) %				
C	H	O	N	S
78.11	5.49	9.81	1.36	4.83

Table 5.3 Composition of coal volatiles (%)

Tar	CH$_4$	CO	CO$_2$	H$_2$	H$_2$O
42.94	13.5	27.2	5.81	3.47	7.08

For the investigation of MILD combustion, the steady laminar flamelet and perfectly-stirred reactor models are applied. Air at 1200 K is used as undiluted oxidizer. The mixture of volatile light gases (with composition of CH$_4$, CO, CO$_2$, H$_2$ and H$_2$O as shown in Table 5.3) and reaction products of tar and soot oxidation (with composition of CO, H$_2$O and N$_2$) is used as fuel stream. Its composition and temperature are calculated using Eqs. (5.27) and (5.29). The adiabatic equilibrium product of stoichiometric air and fuel stream is used as the recirculated flue gas, and the recirculation rate in Eq. (5.34) is calculated based on the mass flow rate of stoichiometric air and fuel stream.

5.4 Results and Discussion

5.4.1 Comparison of Mixture Fraction-Based Models

In this section, the a priori performance of the Burke-Schumann (BS), equilibrium (EQ), and steady laminar flamelet (SLF) models is evaluated using data from a turbulent coal combustion simulation in which a detailed kinetics (DK) model for chemistry is implemented. Because soot is assumed to have the same empirical formula as tar and both differential diffusion and speciation are neglected, differences between simulation data and model reconstructions should be due only to variations in the chemical and diffusive time scales. Herein, use of "expected" or "observed" data refers to that originating from detailed kinetics calculations.

Figure 5.1 shows model reconstructions of T_g using the Burke-Schumann, equilibrium, and flamelet models in addition to T_g from simulation data plotted against equivalence ratio and colored by heat loss. As Fig. 5.1 indicates, the accuracy of model reconstructions of T_g greatly depends on model fidelity. The Burke-Schumann model yields temperature reconstructions that overestimate T_g by almost 600 K near stoichiometric conditions. Reconstruction of gas temperature by the equilibrium model also overestimates the expected temperature in the vicinity of $\phi = 1$, though is substantially more accurate the Burke-Schumann reconstruction of T_g. Additionally, flamelet reconstructions of T_g very closely resemble values obtained from simulation data. Figure 5.2 shows model reconstructions of Y_{O_2} as well as values obtained from simulation data plotted against equivalence ratio and colored by heat loss. As Fig. 5.2 indicates, reconstructions of Y_{O_2} mirror the expected behavior when $\phi < 0.5$ for all models considered. However, the behavior of Y_{O_2} is model-dependent for larger ϕ. For $\phi > 0.5$, the Burke-Schumann model underpredicts Y_{O_2} values from

Fig. 5.1 Gas temperature, T_g, plotted against equivalence ratio, ϕ, for the detailed kinetics (DK), Burke-Schumann (BS), equilibrium (EQ), and flamelet (SLF) models. Data colored according to the scale of the color bar is set based on normalized heat loss, γ
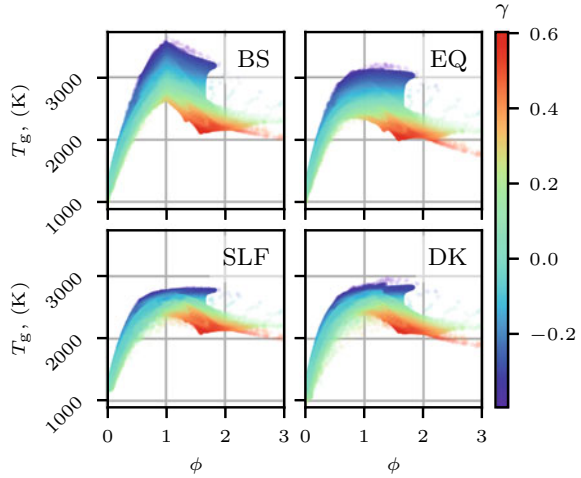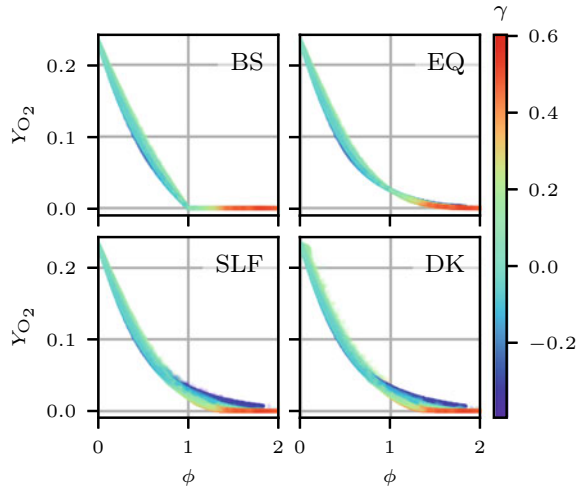

Fig. 5.2 Oxygen mass fraction, Y_{O_2}, plotted against equivalence ratio, ϕ, for the detailed kinetics (DK), Burke-Schumann (BS), equilibrium (EQ), and flamelet (SLF) models. Data colored according to the scale of the color bar is set based on normalized heat loss, γ


the simulation data. Underestimation of Y_{O_2} by the Burke-Schumann model is especially egregious under stoichiometric conditions where it predicts $Y_{O_2} = 0$, which is a consequence of the "mixed is burnt" assumption. Unlike the Burke-Schumann model, equilibrium chemistry produces a Y_{O_2} profile that is nearly identical to values obtained from simulation data for sufficiently lean conditions, ($\phi < 0.8$) and matches the general trend of Y_{O_2} for larger ϕ, but fails to capture the observed variance. Similar to the equilibrium model the flamelet reconstruction of Y_{O_2} mirrors values from simulation data under lean conditions. Additionally, the flamelet model is able to reproduce the expected behavior of Y_{O_2} at and near stoichiometric conditions which neither the Burke-Schumann nor equilibrium models are able to do.

Fig. 5.3 Oxygen mass fraction, Y_{CO}, plotted against equivalence ratio, ϕ, for the detailed kinetics (DK), Burke-Schumann (BS), equilibrium (EQ), and flamelet (SLF) models. Data colored according to the scale of the color bar is set based on normalized heat loss, γ
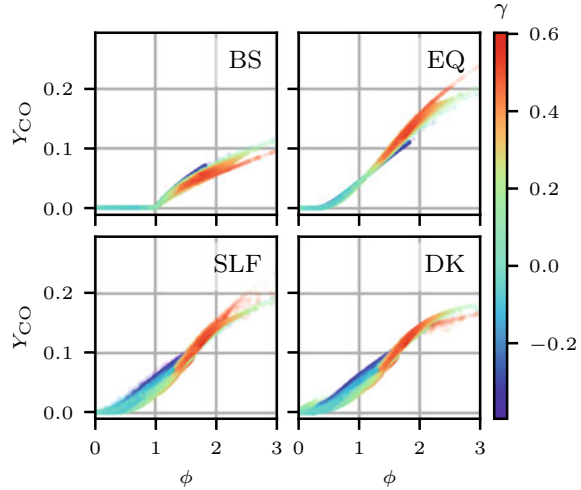
Figure 5.3 shows model reconstructions of Y_{CO} in addition to data originating from detailed kinetics calculations plotted against equivalence ratio and colored by heat loss. As is observed with T_g and Y_{O_2}, the accuracy of predicted Y_{CO} varies substantially among the models considered. For instance, the Burke-Schumann model significantly underestimates Y_{CO} for nonzero ϕ, but both the equilibrium and flamelet models yield predictions that match the general behavior of Y_{CO} obtained from simulation data. Additionally, both the equilibrium and flamelet models tend to overestimate Y_{CO} when $\phi > 2$ and $\gamma > 0.4$, though the flamelet model overestimates by a smaller margin. As observed with Y_{O_2}, the equilibrium model is unable to reproduce the variance in Y_{CO} for fixed ϕ, under lean conditions, whereas the flamelet reconstruction of Y_{CO} are almost indistinguishable from expected values.

Figure 5.4 shows of T_g, Y_{O_2}, and Y_{CO} as predicted by the Burke-Schumann, equilibrium, and steady laminar flamelet models plotted against values obtained from simulation data. Data in Fig. 5.4 are colored by ϕ. As Fig. 5.4 illustrates, the flamelet model generally reproduces expected values of T_g, Y_{O_2}, and Y_{CO} more accurately than both the equilibrium and Burke-Schumann models. The only exception to this generalization is T_g at $\phi \approx 0$, where T_g as predicted by the flamelet model approaches 1200 K as ϕ approaches 0. As mentioned in Sect. 5.2.2.3, non-adiabatic flamelets are generated by including a source term on the right-hand side of the energy conservation equation (Sect. 5.2.2.3) while maintaining adiabatic boundary conditions. Consequently, this method of generating non-adiabatic flamelets cannot resolve heat loss at mixture fraction boundaries, which is the cause of the errant behavior of the flamelet temperature at $\phi \approx 0$. It is also evident from Fig. 5.4 that, for the dataset considered, the accuracy of equilibrium reconstructions is typically close to that of flamelet reconstructions. Furthermore, Fig. 5.4 illustrates the poor accuracy of Burke-Schumann the model for predicting T_g, Y_{O_2}, and Y_{CO}. Accurate Burke-Schumann
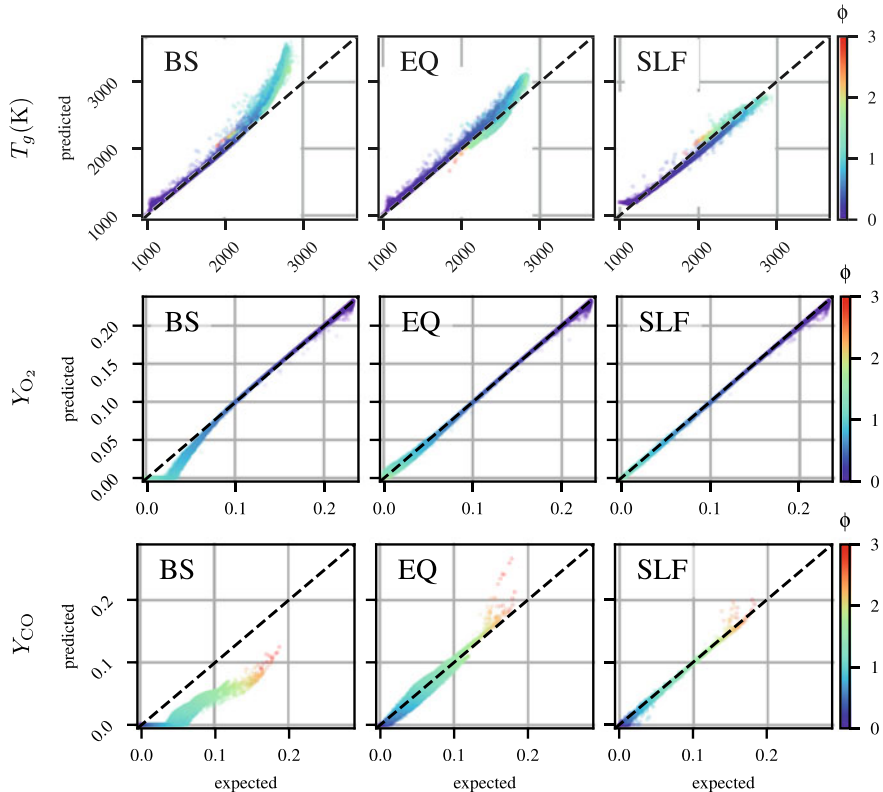
Fig. 5.4 Parity plots of a priori predictions of gas temperature (top row), O_2 mass fraction (middle row) and CO mass fraction (bottom row) given by the Burke-Schumann (left column), equilibrium (middle column), and steady laminar flamelet (right column) models

reconstructions for T_g and Y_{O_2} are limited to $\phi < 0.5$, while the Y_{CO} reconstruction is inaccurate for $\phi > 0$.

5.4.2 Analysis of MILD Combustion Using Well-Stirred Reactor and Steady Flamelet Models

From the analysis in Sect. 5.4.1, the steady flamelet model is significantly more accurate than both the equilibrium and Burke-Schumann models, especially considering predictions of T_g. Therefore, it is applied to investigate the MILD combustion behavior and is compared with the well-stirred reactor model.

To achieve MILD combustion and test the effect of dilution rate, we vary the recirculation rate (K_v). Five values of K_v, namely 0.0, 0.5, 1.0, 1.5 and 2.0, are used

in this work. From the analysis in Sect. 5.4.1, $\gamma = -0.2$, 0.0 and 0.4 are obtained for normalized heat loss. The negative heat loss indicates that the gas phase absorbs energy from surroundings or particles. The positive heat loss indicates that the gas phase releases energy to surroundings or particles. $\zeta = 0.10, 0.25, 0.40$ and 0.80 are used for mass fraction of light gases.

In both steady flamelet and well-stirred reactor models, temperatures for the light gas (lg) and tar and soot reaction product (tp) streams are computed from ODT simulation data, and are $T_{\mathrm{lg}} = 1176K$ and $T_{\mathrm{tp}} = 2380K$, respectively. The mixture of the light gas (lg) and tar and soot reaction product (tp) streams are used as fuel. The mixture of recirculated flue gases and undiluted oxidizer (air) are used as oxidizer. Its temperature and composition are calculated based on the value of K_v. For the well-stirred reactor model, the inflow conditions are obtained by mixing fuel and diluted oxidizer under constant pressure and enthalpy, whose temperature is used as the inlet temperature, T_{inlet}. A long residence time, $\tau_{\mathrm{mix}} = 10^3$s, is applied. For flamelet model, different dissipation rates in the range of $10^{-2} \leq \chi_{\mathrm{max}} \leq 2 \times 10^4$ are tested.

Based on the temperature criterion for MILD combustion, $T_{\mathrm{inlet}} > T_{\mathrm{ignition}}$ and $\Delta T < T_{\mathrm{ignition}}$, with $\Delta T = T_{\mathrm{max}} - T_{\mathrm{inlet}}$ (Cavaliere and De Joannon 2004), the maximum and inlet temperatures for various K_v, γ and ζ with equivalence ratio $\phi = 1$ from the well-stirred reactor model are compared in Fig. 5.5. The maximum temperature, T_{max}, decreases with the increment of heat loss, γ, as indicated by three red lines in each sub-figure, while the inlet temperatures, T_{inlet}, are the same for various heat losses. This results in the decrease of the disparity between T_{max} and T_{inlet}, which is helpful for achieving MILD combustion. Also, T_{inlet} decreases as ζ increases because T_{lg} is significantly less than T_{tp}, while T_{max} does not change much for different ζ. This indicates that having more production of tar and soot oxidation in the fuel stream makes it easier to achieving MILD regime. For different recirculation rate K_v, T_{inlet} increases significantly for bigger K_v because of the high temperature of recirculated flue gas. For $\gamma = 0.0$, T_{max} keeps constant for various K_v because the recirculated flue gas has the same composition and temperature as the gas phase in the PSR without recirculation. The recirculated flue gas only increases T_{inlet} and does not have any effects in the reactor due to the well-mixed reactants within the reactor. When γ is not zero, the products, from the *adiabatic* stoichiometric reaction, are different from the gas phase in the PSR, leading to the variance of T_{max}. For large K_v, the adiabatic and reference enthalpy, h_{ad} and $h(T_{\mathrm{g,ref}})$, in Eq. (5.19) increase due to bigger amount of flue gas, which results in bigger heat loss ($h_{\mathrm{ad}} - h_{\mathrm{sim}}$) with the same γ. Therefore, T_{max} decreases for $\gamma = 0.4$ and increases for $\gamma = 0.2$ with the increment of K_v.

Figure 5.6 delineates the combustion regimes as the right bottom area based on the definition of MILD combustion. Three subplots respond to different heat loss values, while different symbols respond to different mass fractions of light gases in fuel stream. In this work, the undiluted oxidizer(air) is preheated to 1200 K. The combustion drops into the *High Temperature Combustion* area when $K_v = 0$. With the increment of K_v, the combustion moves from *High Temperature Combustion* area to *MILD Combustion* area. The heat loss value does have effect on the achievement
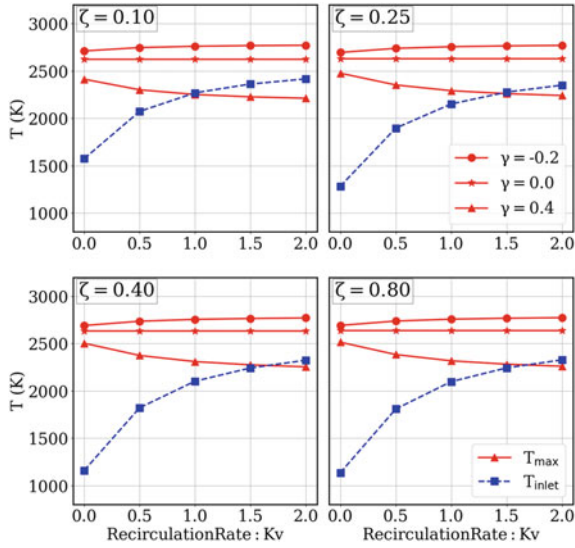
Fig. 5.5 Variances of inlet and maximum temperatures for different K_v, γ and ζ with equivalence ratio $\phi = 1$ from well-stirred reactor model
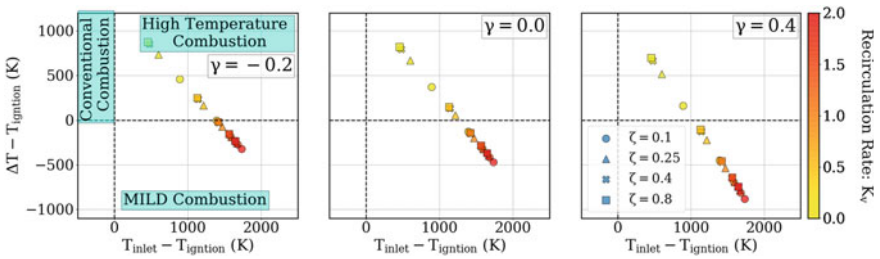

Fig. 5.6 The effect of recirculation rate on determining combustion regimes for different γ and ζ from well-stirred reactor model. Data colored according to the scale of the color bar is set based on recirculation rate, K_v

of MILD combustion. For adiabatic conditions ($\gamma = 0$), MILD is achieved for all ζ when $K_v \geq 1.0$, while it only requires $K_v \geq 0.5$ for positive heat loss, $\gamma = 0.4$. For negative heat loss, $\gamma = -0.2$, it requires $K_v \geq 1.0$ for $\zeta < 0.8$. The case with $\zeta = 0.8$ and $\gamma = -0.2$ is on the edge between *High Temperature Combustion* and *MILD Combustion* area for $K_v = 1.0$. When ζ is decreased for the same value of K_v, the state of the system moves closer to the *MILD Combustion* area due to the higher temperature of the production of tar and soot oxidation as indicated in Fig. 5.5. From the analysis of Figs. 5.5 and 5.6, it is concluded that higher recirculation K_v, elevated heat loss γ and lower mass fraction of light gas in fuel stream ζ are helpful to reach MILD regime.

Fig. 5.7 Gas temperature, T_g, plotted against equivalence ratio, ϕ, for various recirculation rates, K_v, with no heat loss, $\gamma = 0$, and $\zeta = 0.4$. Data are colored according to the scale of the color bar based on dissipation rate, χ_{max}
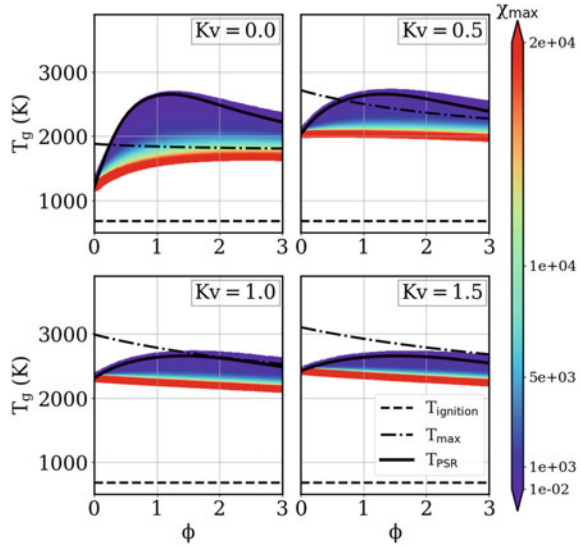
Figures 5.7, 5.8 and 5.9 compare the results from well-stirred reactor and flamelet models for for several values of K_v with $\zeta = 0.4$. Each figure gives the results for a single heat loss. The region between the black dashed line and dot-dash line represents the region where MILD combustion is achieved. The bottom dashed line indicates the mixture self-ignition temperature. The top dash-dot line indicates the maximum allowable temperature, $T_{max} = T_{inlet} + T_{ignition}$, of MILD combustion. The black solid line is the result from well-stirred reactor. The data from the flamelet model is colored based on the value of the dissipation rate, χ_{max}.

For the results from PSR (solid black lines in the figures) with no recirculation ($K_v = 0.0$), the temperature far exceeds the allowable maximum temperature for the three heat loss values considered, especially near stoichiometric, indicating that MILD regime is not achieved. When ϕ is smaller than $\sim$0.5, the temperature drops into the MILD regime between two black dashed lines. That is, only when the the stoichiometry is very lean can MILD be achieved in PSR with no recirculation. As K_v increases, the allowable maximum temperature, T_{max}, increases due to increasing inlet temperature, T_{inlet}. The MILD regime between two black dashed lines becomes much larger. The range of equivalence ratios for achieving MILD regime becomes bigger for larger K_v until the entire black line drops into the MILD regime with $K_v = 1.0$ for $\gamma = 0.0$ and with $K_v = 0.5$ for $\gamma = 0.4$. For $\gamma = -0.2$, cases with $\phi > 1.5$ cannot reach the MILD regime even for $K_v = 1.5$.

For the results from steady flamelet model, the temperatures are almost the same as the results from PSR for small dissipation rate, $\chi_{max} = 10^{-2}$. As dissipation rate increases, temperature decreases and drops into the MILD regime for all equivalence ratios of 0.0−3.0 when χ_{max} is sufficiently large. The required dissipation rate to achieve MILD combustion for all equivalence ratios of 0.0−3.0 is referred to as

Fig. 5.8 Gas temperature, T_g, plotted against equivalence ratio, ϕ, for different recirculation rates, K_v, with negative heat loss, $\gamma = -0.2$, and $\zeta = 0.4$. Data are colored according to the scale of the color bar based on dissipation rate, χ_{max}
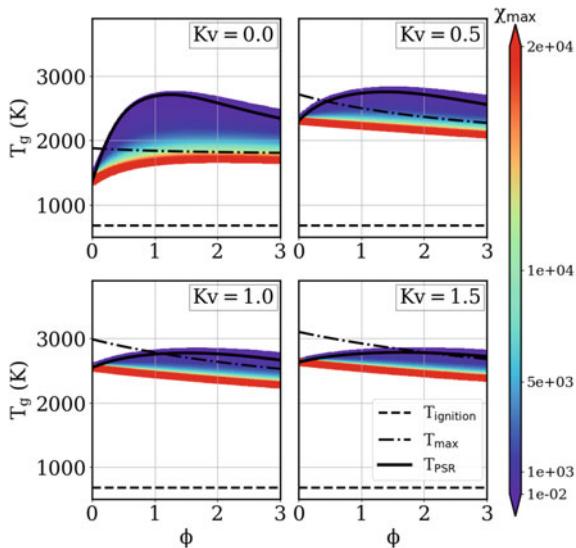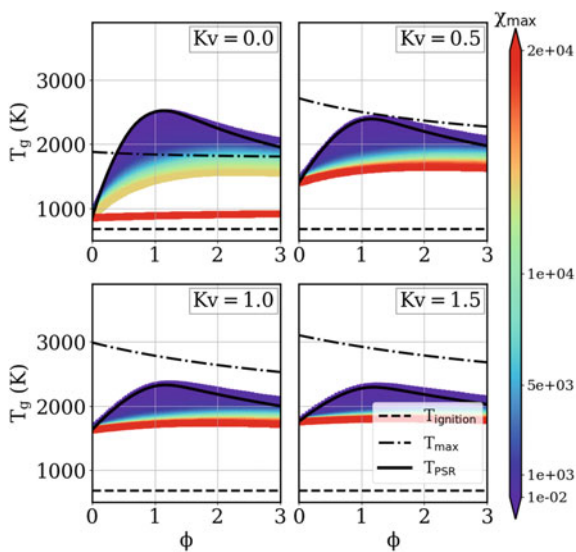
Fig. 5.9 Gas temperature, T_g, plotted against equivalence ratio, ϕ, for different recirculation rates, K_v, with positive heat loss, $\gamma = 0.4$, and $\zeta = 0.4$. Data colored according to the scale of the color bar is set based on dissipation rate, χ_{max}

$\chi_{max,MILD}$. For $K_v = 0.0$, $\chi_{max,MILD}$ is around 1.5×10^4 for the adiabatic case ($\gamma = 0$) and for $\gamma = -0.2$, while it is approximately 1.0×10^4 for $\gamma = 0.4$. However, extinction is observed for the case with $K_v = 0.0$ and $\gamma = 0.4$ when the dissipation rate reaches $\sim 1.5 \times 10^4$. That is, a maximum dissipation rate should also been considered to avoid extinction. $\chi_{max,MILD}$ decreases with the increment of recirculation rate. When $K_v = 1.5$ for $\gamma = 0$ and $K_v = 0.5$ for $\gamma = 0.4$, MILD regime is achieved for all dissipation rates in $10^{-2} - 2 \times 10^4$.

Fig. 5.10 Gas temperature, T_g, plotted against equivalence ratio, ϕ, for different mass fractions of light gas in fuel stream, ζ, with no heat loss, $\gamma = 0.0$ and no recirculation $K_v = 0.0$. Data colored according to the scale of the color bar is set based on dissipation rate, χ_{max}
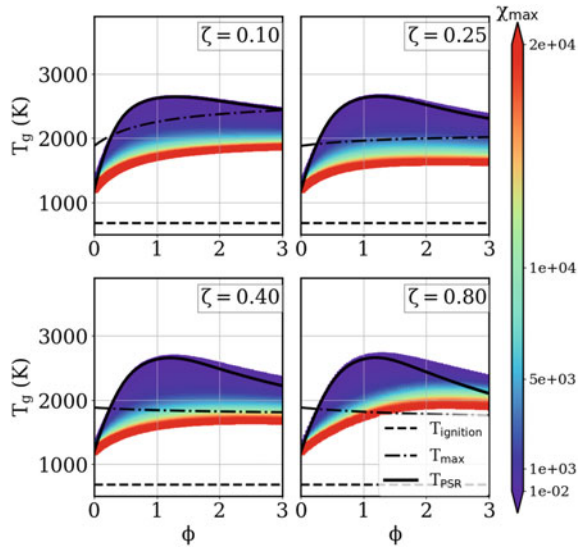
The light gases and products of tar and soot oxidation are generated under different temperatures, and will affect the inlet temperature T_{inlet} as shown in Fig. 5.5. In order to evaluate its effect, gas temperatures from PSR and steady flamelet model are plotted against equivalence ratio in Fig. 5.10 with $K_v = 0.0$ and $\gamma = 0.0$. Figure 5.5 indicates a decrease of inlet temperature for large values of ζ, which causes the decrease of the maximum allowable temperature for the MILD combustion regime. As a result, the required dissipation rate, $\chi_{max,MILD}$, to achieve MILD regime increases for bigger ζ.

5.5   Conclusions

In this study, we carry out an a priori analysis of three mixture fraction-based chemistry models. Data used as a basis for assessing model performance was generated from a one-dimensional turbulent coal combustion simulation in which detailed kinetics is implemented for gas phase chemistry. This work only considers devolatilization; neither char combustion nor evaporation are accounted for. Furthermore, tar and soot are considered through an approach based on Brown-Fletcher tar and soot model. Soot is assumed to have the same empirical formula as tar in order to facilitate the two mixture fraction parameterization of the system composition.

Of the three mixture fraction-based approaches considered, the flamelet model performed the best. Flamelet reconstructions for T_g, Y_{O_2}, and Y_{CO} were typically very accurate. This is especially the case for T_g near stoichiometric conditions where the Burke-Schumann and equilibrium models struggle to be accurate. However, the accuracy of T_g predictions by the flamelet model declines for $\phi \approx 0$ because the

approach used is to generate non-adiabatic flamelets is not capable of resolving heat loss at mixture fraction boundaries. The accuracy of equilibrium reconstructions was often close to those of the flamelet model, although the equilibrium predictions of temperature were typically off by 150 K at stoichiometric conditions. The Burke-Schumann model was the least accurate of the three models considered, performing very poorly for T_g, Y_{O_2}, and Y_{CO} under stoichiometric conditions.

To investigate the MILD combustion behavior, the steady flamelet model and well-stirred reactor model are applied in this work. The definition of MILD combustion based on temperature relationship, $T_{inlet} > T_{ignition}$ and $\Delta T < T_{ignition}$, with $\Delta T = T_{max} - T_{inlet}$, is applied as the criteria for achieving MILD combustion. The effects of three main parameters, including recirculation rate, K_v, normalized heat loss, γ, and mass fraction of light gases in fuel stream, ζ, are evaluated for MILD combustion. Increasing recirculation rate, positive heat loss and decreasing mass fraction of light gases in fuel steam have positive influence on attaining of MILD combustion. Negative heat loss and increasing light gases mass fraction in fuel stream increases the critical value of recirculation rate needed to achieve MILD regime. The dissipation rate plays important role in achieving MILD combustion. For instance, the MILD regime can be achieved with higher dissipation rate under poorly-mixed combustion , and its critical value decreases as the recirculation rate or heat loss increase and as mass fraction of light gas in fuel stream decreases. In other words, flamelet model provides a reliable method to model MILD regime with high dissipation rate in diffusion combustion.

References

Bai Y, Luo K, Qiu K, Fan J (2016) Numerical investigation of two-phase flame structures in a simplified coal jet flame. Fuel 182:944–957. ISSN: 0016-2361

Brown AL, Fletcher TH (1997) Modeling soot derived from pulverized coal. Energy Fuels 4:745–757

Burke SP, Schumann TEW (1928) Diffusion flames. Ind Eng Chem 20:998–1004

Cavaliere A, De Joannon M (2004) Mild combustion. Prog Energy Combust Sci 30:329–366

Goodwin DG, Moffat HK, Speth RL (2017) Cantera: an object-oriented software toolkit for chemical kinetics, thermodynamics, and transport processes version 2.3.0. https://doi.org/10.5281/zenodo.170284. http://www.cantera.org

Goshayeshi B, Sutherland JC (2015a) Prediction of oxy-coal flame stand-off using high-fidelity thermochemical models and the one-dimensional turbulence model. Proc Combust Inst 35:2829–2837. ISSN: 15407489

Goshayeshi B, Sutherland JC (2015b) A comparative study of thermochemistry models for oxy-coal combustion simulation. Combust Flame 162:4016–4024. ISSN: 0010-2180

Goshayeshi B, Sutherland JC (2019) A comparison of various models in predicting ignition delay in single-particle coal combustion. Combust Flame 161:1900–1910. ISSN: 15562921 (2014). In: 9th International symposium on coal combustion (ISCC-9) Qingdao, China, 21–24 July 2019

Hansen MA, Sutherland JC (2017) Dual timestepping methods for detailed combustion chemistry. Combusti Theory Model Month 21:329–345

Hara T, Muto M, Kitano T, Kurose R, Komori S (2015) Direct numerical simulation of a pulverized coal jet flame employing a global volatile matter reaction scheme based on detailed reaction mechanism. Combust Flame 162:4391–4407. ISSN: 0010-2180

Jupudi R, Zamansky V, Fletcher T (2009) Prediction of light gas composition in coal devolatilization. Energy Fuels 23:3063–3067

Kerstein AR (1999) One-dimensional turbulence: model formulation and application to homogeneous turbulence, shear flows, and buoyant stratified flows. J Fluid Mech 392:277–334

Li P et al (2014) Moderate or intense low-oxygen dilution oxy-combustion characteristics of light oil and pulverized coal in a pilot-scale furnace. Energy Fuels 28:1524–1535. ISSN: 08870624

Lu T, Law CK (2008) A criterion based on computational singular perturbation for the identification of quasi steady state species: a reduced mechanism for methane oxidation with NO chemistry. Combust Flame 154:761–774. ISSN: 00102180

Luo K, Wang H, Fan J, Yi F (2012) Direct numerical simulation of pulverized coal combustion in a hot vitiated co-flow. Energy Fuels 26:6128–6136

McConnell J, Sutherland JC (2020) Assessment of various tar and soot treatment methods and a priori analysis of the steady laminar flamelet model for use in coal combustion simulation. Fuel 265:116775. ISSN: 00162361

McConnell J, Goshayeshi B, Sutherland JC (2016) The effect of model fidelity on prediction of char burnout for single-particle coal combustion. Proc Combust Inst

McConnell J, Goshayeshi B, Sutherland JC (2017) An evaluation of the efficacy of various coal combustion models for predicting char burnout. Fuel 201:53–64

Olenik G, Stein O, Kronenburg A (2015) LES of swirl-stabilised pulverised coal combustion in IFRF furnace No. 1. Proc Combust Inst 35:2819–2828. ISSN: 1540-7489

Özdemir IB, Peters N (2001) Characteristics of the reaction zone in a combustor operating at mild combustion. Exp Fluids 30:683–695. ISSN: 07234864

Pedel J, Thornock JN, Smith PJ (2013) Ignition of co-axial turbulent diffusion oxy-coal jet flames: experiments and simulations collaboration. Combust Flame 160:1112–1128. ISSN: 0010-2180

Peters N (1984) Laminar diffusion flamelet models in non-premixed turbulent combustion. Prog Energy Combust Sci 10:319–339. ISSN: 0360-1285

Plessing T, Peters N, Wünning JG (1998) Laseroptical investigation of highly preheated combustion with strong exhaust gas recirculation. Symp (Int) Combust 27:3197–3204. ISSN: 00820784

Rieth M et al (2016) Flamelet LES of a semi-industrial pulverized coal furnace. Combust Flame 173:39–56. ISSN: 0010-2180

Rieth M, Kempf A, Kronenburg A, Stein O (2018) Carrier-phase DNS of pulverized coal particle ignition and volatile burning in a turbulent mixing layer. Fuel 212:364–374. ISSN: 0016-2361

Saha M, Dally BB, Medwell PR, Cleary E (2013) An experimental study of MILD combustion of pulverized coal in a recuperative furnace 2 experimental setup. In: 9th Asia-Pacific conference on combustion, Gyeongju Hilton, Gyeongju, Korea, 19–22 May 2013, pp 3–6

Saha M, Dally BB, Medwell PR, Cleary EM (2014) Moderate or intense low oxygen dilution (MILD) combustion characteristics of pulverized coal in a self-recuperative furnace. Energy Fuels 28:6046–6057. ISSN: 15205029

Saha M, Chinnici A, Dally BB, Medwell PR (2015) Numerical study of pulverized coal MILD combustion in a self-recuperative furnace. Energy Fuels 29:7650–7669. ISSN: 15205029

Saha M, Dally BB, Medwell PR, Chinnici A (2016) Burning characteristics of Victorian brown coal under MILD combustion conditions. Combust Flame 172:252–270. ISSN: 15562921

Saha M, Dally BB, Medwell PR, Chinnici A (2017) Effect of particle size on the MILD combustion characteristics of pulverised brown coal. Fuel Process Technol 155:74–87. ISSN: 03783820

Smart JP, Riley GS (2012) Combustion of coal in a flameless oxidation environment under oxyfuel firing conditions: the reality. J Energy Inst 85:131–134

Suda T, Takafuji M, Hirata T, Yoshino M, Sato J (2002) A study of combustion behavior of pulverized coal in high-temperature air. Proc Combust Inst 29:503–509. ISSN: 1540–7489

Sutherland JC, Kennedy CA (2003) Improved boundary conditions for viscous, reacting, compressible flows. J Comput Phys 191:502–524. ISSN: 00219991

Sutherland J, Punati N, Kerstein A (2019) A unified approach to the various formulations of the one-dimensional-turbulence model tech. rep. (Inst. Clean Secure Energy, 2010). In: 9th International symposium on coal combustion (ISCC-9), Qingdao, China, 21–24 July 2019

Tamura M, Watanabe S, Komaba K, Okazaki K (2015) Combustion behaviour of pulverised coal in high temperature air condition for utility boilers. Appl Thermal Eng 75:445–450

Watanabe J, Yamamoto K (2015) Flamelet model for pulverized coal combustion. Proc Combust Inst 35:2315–2322. ISSN: 1540-7489

Watanabe J, Okazaki T, Yamamoto K, Kuramashi K, Baba A (2017) Large-eddy simulation of pulverized coal combustion using flamelet model. Proc Combust Inst 36:2155–2163. ISSN: 1540-7489

Weber R, Smart JP, Kamp WV (2005) On the (MILD) combustion of gaseous, liquid, and solid fuels in high temperature preheated air. Proc Combust Inst 30(II):2623–2629. ISSN: 15407489

Wen X, Wang H, Luo K, Fan J (2019) Analysis and flamelet modelling for laminar pulverised coal combustion considering the wall effect. Combust Theory Model 23:353–375

Wunning JA, Wunning JG (1997) Flameless oxidation to reduce thermal NO-formation. Prog Energy Combust Sci 23(23):81–94

Zhao Y, Serio MA, Bassilakis R, Solomon PR (1994) A method of predicting coal devolatilization behavior based on the elemental composition. Symp (Int) Combust 25:553–560. ISSN: 0082-0784

Zhou MM et al (2019) Large-eddy simulation of ash deposition in a large-scale laboratory furnace. Proc Combust Inst 37:4409–4418. ISSN: 15407489